Macro-Mini Actuation of Pneumatic Pouches for Soft Wearable Haptic Displays

Brian H. Do[1], Allison M. Okamura[1], Katsu Yamane[2], Laura H. Blumenschein[3]

Abstract— Pneumatic wearable haptic devices can provide distributed pressure feedback to human operators during robot teleoperation and in virtual and augmented reality. However, these devices have an inherent trade-off between the spatial coverage of their pressure output and their resolution and dynamic response. To achieve specified spatial resolution and dynamic response, we propose a macro-mini actuation approach that stacks a number of smaller inflatable pouches atop a larger inflatable pouch. We develop models for the static and dynamic responses of single and stacked pouches and compare these with experimental results, providing guidelines for the design of wearable stacked pneumatic displays. Finally, we demonstrate this pneumatic macro-mini approach by replicating the time series pressure profiles of data collected from a huggable robot embedded with distributed force sensors.

I. INTRODUCTION

Novel forms of haptic (force and tactile) feedback are being created to enable physical interactions between humans and robots or virtual/augmented reality environments. Haptic devices have been made in a variety of form factors, with most involving the use of our hands. The limited surface area of the hands combined with the added encumbrance of occupying the hands limits the usefulness of these devices for certain applications. Wearable haptic interfaces with distributed contact area on the skin offer an opportunity to create large-scale haptic stimuli to replicate many interactions we have with the world around us and serve as more intuitive human-robot interfaces. This haptic feedback can provide additional sensory feedback for tasks such as navigation or teleoperation, while also keeping the hands unencumbered.

Many past body-grounded haptic devices have provided vibrotactile feedback by distributing embedded actuators in vests [1], [2], jackets [3], [4] or other form factors [5], [6]. While such arrangements enable precise spatial distributions of vibrations, they cannot produce skin compression. In general, there has been comparatively little study of tactile feedback via distributed pressure despite the additional richness it offers in replicating social interactions such as hugging or patting, as well as other external stimuli.

Pneumatic force displays are an attractive option for producing skin compression as well as vibrotactile sensations in a lightweight, conformable form factor. Past work has used pouches embedded in vests, jackets, and soft exoskeletons to render haptic sensations for augmented reality [7], teleoperation [8], motion guidance [9], and remote social touch [10]. Researchers have also used inflatable pouches made of inextensible but flexible material as the basis for soft actuators, such as the pouch motor [11] and the series pneumatic artificial muscle [12], by exploiting the shape change that occurs during the inflation process to produce contraction or rotation.

Previous pouch-based pneumatic force displays have been controlled through closed-loop feedback on the pouch's internal air pressure or on the force/pressure measured by sensors embedded into the pouch surface. Neither approach is sufficient to encompass the full interaction forces of the pouch. A pouch with low pressure and large contact area can produce the same magnitude of force as a pouch with high pressure and small contact area; however, the physical sensations will be very different. Therefore, to accurately render desired haptic sensations, it is important to control both contact area and applied pressure. Additionally, the inherent dynamics of pneumatic actuation limits their performance. Body-worn haptic systems covering the torso result in large pouch volumes, and the larger the volume to inflate, the slower the dynamic response. One possible solution is to use smaller pouches, which also allows for more targeted haptic sensations and increases the resolution of these pneumatic displays. However, smaller pouches also result in less contact area with the skin compared to larger pouches for the same inflation height. Thus, a trade-off exists between an inflated pouch's contact area and the speed of its dynamic response.

We propose a macro-mini approach to pouch structure. In robotics, the macro-mini actuation approach distributes lighter, lower bandwidth actuators along a manipulator chain anchored at its base by heavier, more powerful motors to optimize overall force output and responsiveness [13]. We propose an analogous division for pneumatic pouches in which smaller pouches that make skin contact are stacked atop larger pouches, allowing finer spatial resolution and faster dynamics while maintaining a large contact area. This macro-mini pouch stacking can be spatially localized and deployed in serial or parallel configurations.

II. SETUP AND EXPERIMENTAL METHODS

In general, pouches can be fabricated from any thin, flexible, inextensible, air-tight material. Here, pouches were created by heat sealing low density polyethylene (LDPE) plastic tubes due to ease of fabrication. To allow airflow into pouches, nylon through-wall connectors were embedded

[1]Department of Mechanical Engineering, Stanford University, Stanford, CA 94305 USA {`brianhdo, aokamura`}`@stanford.edu`

[2]Honda Research Institute, San Jose, CA 95134 USA `kyamane@honda-ri.com`

[3]School of Mechanical Engineering, Purdue University, Lafayette, IN 47901, USA. `lhblumen@purdue.edu`
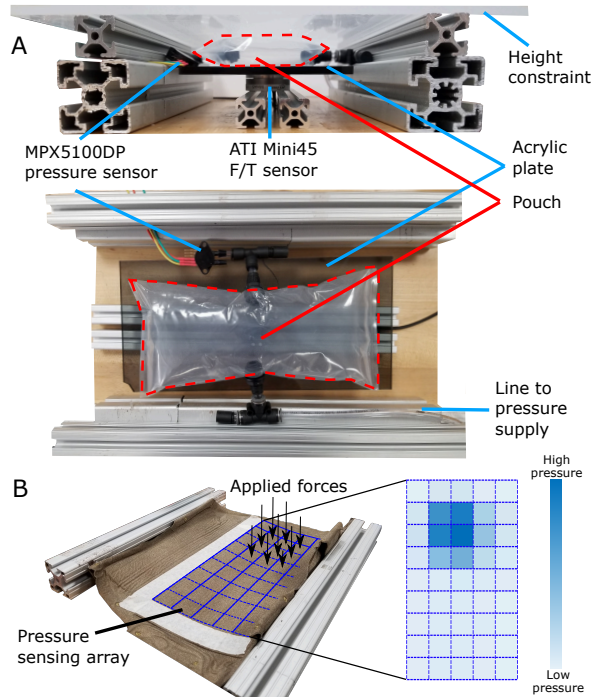
Fig. 1. (A) Side and top views of testing setup with pressure and force sensing. (B) Pressure sensing array with 2.54 cm×2.54 cm capacitive cells. Grid lines marking the boundary of each cell are shown in blue, and an example pressure distribution is shown to the right.

into the pouch walls. One side was connected to a pressure source, and the opposite side was connected to a pressure sensor (NXP MPX5100DP). Closed-loop pressure control was achieved using Proportion Air QB3 regulators. For tests investigating the pouch dynamic response to a step pressure input, air was supplied from a large pressure chamber to provide near constant pressure after opening a valve in order to avoid including the pressure regulator internal dynamics.

Two experimental setup variants were used to measure the dynamic and static characteristics of the pouches. In the first, shown in Fig. 1(A), pouches were placed on top of an acrylic plate mounted to an ATI Mini45 Force/Torque sensor. This was used for the dynamic experiments. In the second, shown in Fig. 1(B), static spatial force distributions were recorded by placing pouches on a custom soft pressure sensing array (Pressure Profile Systems). The rectangular 580 cm^2 array is composed of 2.54 cm×2.54 cm capacitive sensors.

For both test setups, a height constraint, h, was imposed on the pouch. A flat plate secured by weights was placed above the pouch at the desired height set by aluminum framing, which was added or removed to modify the height.

III. FORCE DISTRIBUTION

A. Simplified Pouch Contact Area Model for Design

The total force exerted by a pneumatic pouch on its environment is the product of its contact area and its internal pressure. If the membrane elastic energy is negligible, even a small pressure difference relative to atmosphere will result in inflation to a final volume-maximizing shape that remains

the same even as the internal pressure increases. Thus, to calculate the shape, and therefore the contact area, we only need to consider the geometry and not the pressure.

In general, calculating the shape created by inflating an inextensible membrane is a challenging problem. For rectangular pouches, this has been described as the "paper bag" problem [14]. While inflated shapes in the unconstrained case can be described via calculus of variations by a set of three simultaneous partial differential equations, solving for that shape is considerably complex [15], [16]. Numerical techniques such as finite element modeling can also be used to solve for the shape but are computationally expensive.

Instead, we create a simplified pouch contact area model based on geometric constraints. The model assumes that the uninflated pouch has two flat rectangular faces (length L and width W) made of a flexible, inextensible membrane. Observing real pouches reveals that all sides of this initial rectangle exhibit some curvature in the final inflated pouch shape. We make the simplification that the long sides of the pouch remain straight; that is, we assume that the curvature is sufficiently low that we can treat these sides as straight in order to only consider the relatively higher curvature of the shorter sides. For modeling a square pouch, we arbitrarily treat one set of sides as curving and the other set as straight. The model considers only the gross pouch shape. In reality, when inflated, the pouch surface exhibits a number of small wrinkles that warp the pouch surface. Finally, the model assumes that the pouch is sandwiched between two flat, rigid plates that are separated by a fixed height, h.

In general, the actual shape adopted by a pouch minimizes its potential energy, tending to increase volume and reduce membrane tension. To solve for the shape, the model examines lengthwise cross sections and solves for their dimensions using a set of geometric constraints. Fig. 2(A) shows such a cross section, consisting of a rectangle with elliptical arcs on two sides. The rectangle is defined by h and the length d that the pouch makes contact with the surface. The ellipses have a semi-major axis a and a fixed semi-minor axis $b = \frac{h}{2}$.

Fig. 2(B) shows a top-down pouch view. We assume that the curved sides form an arc with a constant radius of
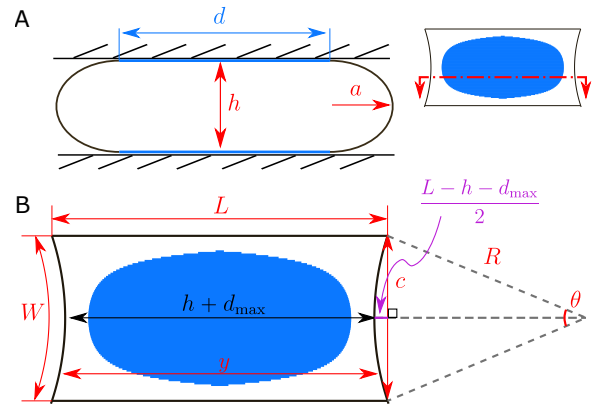

Fig. 2. (A) A side cross section of an inflated pouch. (B) A top-down schematic of a simplified height-constrained inflated pouch.

curvature and an arc length W. As we move towards the middle of W, the projected distance y between these arcs decreases, resulting in the contact length d increasing in order to satisfy the constraint of constant cross-section perimeter.

At the cross section defined by $y_{\min}$ (and thus $d_{\max}$), we assume that the arcs which form the sides of Fig. 2(A) are circular arcs with radius $r = \frac{h}{2}$. Therefore, $y_{\min} = d_{\max} + h$, and the difference between L and each side wall at this point is $(L - h - d_{\max})/2$. Also, since the sides are circular arcs, $\theta = W/R$. Plugging these values into the formula for chord height yields:

$$\frac{1}{2}(L - d_{\max}) - r = R\left(1 - \cos\frac{W}{2R}\right) \qquad (1)$$

Solving (1) for R then allows us to calculate the chord length $c = 2R\sin\frac{\theta}{2}$. This value then gives the pouch corner locations, which, along with R, specify the equations of the circles that define the side arcs seen from the top-down projected view of the pouch in Fig. 2(B). The distance y between the left and right pouch sides can be calculated by taking the difference between the two circle equations.

To solve for d for the rest of the pouch, we use constraints on the projected distance y and cross section perimeter $2L$:

$$y = d + 2a \qquad (2)$$

$$2L = 2d + \pi\left[3\left(\frac{h}{2} + a\right) - \sqrt{\left(3\frac{h}{2} + a\right)\left(\frac{h}{2} + 3a\right)}\right] \qquad (3)$$

Equation (3) is the sum of the flat wall portions and the ellipse formed by the sides. Simultaneously solving (2) and (3) yields d and a for all points where the pouch height is h. By discretizing the pouch length, solving the above set of equations at each point, and then numerically integrating all calculated d, the contact area and shape can be calculated.

B. Single Pouch Results

To investigate our simplified contact model, we conducted experiments using the pressure sensing array to measure the spatial force distribution. We tested combinations of three different pouch geometries and eight height constraints, with internal pouch pressures ranging from 3.4 kPa to 25 kPa. This pressure range corresponded to the minimum output pressure of our controller and just below the pouch burst pressure. Fig. 3 visualizes a selection of recorded forces. We used this spatial force distribution data to obtain the contact area of the pouch for that given condition by dividing the total force recorded by the array by the known internal pouch pressure.

Fig. 3 shows an overlay of the predicted contact area and the numerical value. Three key trends were observed. First, for a pouch of a given geometry, its contact area depends only on the height constraint and not on the internal pouch pressure; across all trials, we found that contact area differed by less than 5.5% across tested pressures. If pouch dimensions and the height constraint are scaled at the same rate, the proportion of the pouch surface in contact remains constant. Second, the applied pressure exerted by a pouch
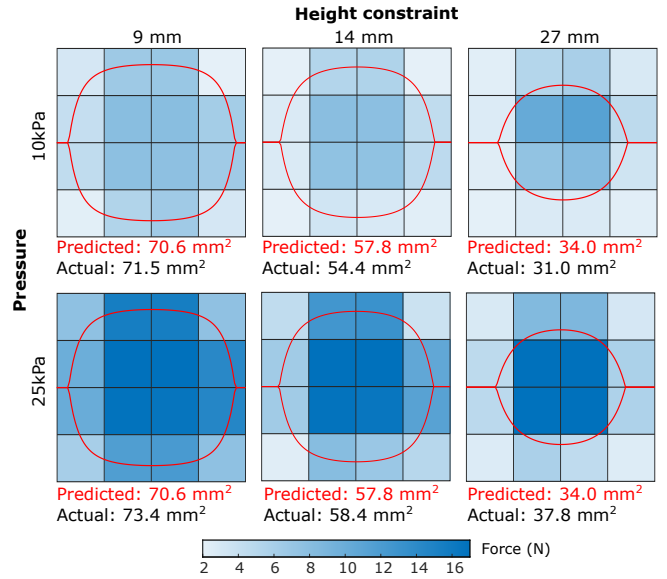

Fig. 3. Spatial force distributions for varied height constraints and pressures for 10.5 cm × 10.5 cm pouches. The predicted and actual contact area is listed beneath each distribution with the predicted shape outlined in red. Contact area remains roughly constant with pressure while varying with the height constraint.

(and thus, the force over any given area) depends directly on its internal pressure. Third, as the height h decreases, the contact area increases.

The error associated with our simplified contact area model increases with aspect ratio (L/W). This is due to only using the lengthwise cross sections of the pouches when solving for a contact area. In reality, the final pouch shape must also satisfy the isoperimetric constraints governing W. Because scaling pouch geometry and the height constraint results in a linear scaling of contact area, we can non-dimensionalize each using aspect ratio, $h^* = h/h_{\max}$, and percent contact area = contact area$/(LW)$, respectively, and use this to calculate the mean absolute percent error (MAPE). From empirical testing, we found that the MAPE from actual contact area measurements for 1:1 aspect ratios was 6.1% for eight tested heights $h^* = [0, 1]$. From testing higher aspect ratios, we found that the height above which the model diverges by more than 10% from measured contact area decreases as the aspect ratio increases. This is due to W becoming the key constraint as the aspect ratio increases and the pouch shape approaches a tube.

C. Stacked Pouches Results

Stacking pouches gives an extra degree of freedom for controlling the total output force by allowing for the contact area to be changed. Fig. 4(A) shows a schematic of the pouch stacking experimental setup using two pouches – one which is proximal to the desired contact surface and the other which is distal to it – stacked on top of each other.

In this arrangement, each pouch can be thought of as a nonlinear spring whose force depends on its internal pouch pressure. The relative ratio of these pressures determines the
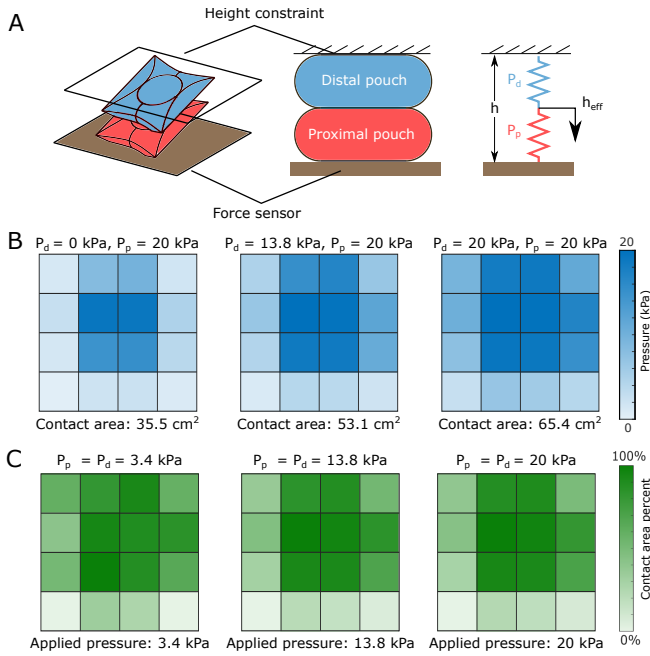
Fig. 4. (A) Schematic views of a sample pouch stacking setup with two pouches. Each pouch can be thought of as a nonlinear spring, and the relative ratios of the two determine the effective height. (B) Pressure distributions for $P_p = 20$ kPa. While the total contact area increases with increasing P_d, the pressure exerted in the middle remains 20 kPa. (C) Contact area distributions show that increasing P_d and P_p by the same relative amount increases the applied pressure while keeping contact area constant.

effective height, h_{eff}, experienced by the proximal pouch.

In a stacked pouch setup, only the pressure of the proximal pouch influences the pressure felt at the contact surface. Fig. 4(B) shows the discretized average pressure recorded by the pressure sensing array when controlling a stacked arrangement with a constant proximal pouch internal pressure $P_p = 20$ kPa and variable distal pouch internal pressure P_d. In all cases, for the center regions where the pouch has complete contact with the force sensing cells, the recorded pressure is 20 kPa. Increasing P_d results in a larger volume filled by the distal pouch. This decreases the effective height of the proximal pouch and thus increases its contact area with the pressure sensing array.

In terms of a force balance, the forces exerted by the proximal and distal pouches must be equal because the stack is constrained between two stationary surfaces. The force each pouch exerts is the product of its contact area and internal pressure. Thus, a lower pressure pouch must have a larger contact area with a surface, and a higher pressure pouch must have a smaller contact area for the total forces to sum to 0. Therefore, the effective height is the value such that the contact areas produced by the proximal pouch at height h_{eff} and the distal pouch at height $h - h_{\text{eff}}$ at their respective surfaces equal in magnitude. The boundary between the pouches has a complex geometry which is a function of the pouch pressure and the membrane stresses. In the case where either $P_d \gg P_p$ or vice versa, the higher pressure pouch fully expands and contacts the opposing surface.

In addition to controlling the contact area while main-

taining a constant applied pressure, we can also control the applied pressure while maintaining a constant contact area. Fig. 4(C) shows how setting $P_d = P_p$ allows us to maintain constant contact area while the applied pressure scales with P_p. Thus, from left to right, the pressure exerted was 3.4 kPa, 13.8 kPa, and 20 kPa. In general, maintaining a constant ratio of $P_d : P_p$ produces a constant contact area.

Therefore, the desired applied pressure determines P_p, and the desired contact area determines h_{eff} and P_d.

IV. DYNAMIC PRESSURE RESPONSE

A. Dynamic Model

In addition to understanding the static force behavior of the pouches, it is important to understand the dynamic behavior of the pressures, and as a result, the forces. To develop a model sufficient to describe the trends and predict the behavior as a function of the geometry and input parameters, we take inspiration from other recent work that use inextensible pouches for haptic interaction. These dynamic models for the pouch pressurization relate the input pressure to the mass of fluid within the pouch and its derivative, mass flow rate. The equations used in our model are adapted from Usevitch et al. and describe the pressurization of inextensible pouches as a combination of the fluidic resistance generated by the hardware between the pressure source and the pouch, and the fluidic capacitance due to the pouch volume [17].

Overall, the dynamic model is:

$$P_i = F_{\text{res}}(\dot{m}) + F_{\text{cap}}(m) \tag{4}$$

where P_i is the input pressure, F_{res} is the fluidic resistance as a function of the mass flow rate, $\dot{m}$, and F_{cap} is the fluidic capacitance as a function of the fluid mass within the pouch, m. Fluidic resistance for a compressible fluid is [18]:

$$F_{\text{res}}(\dot{m}) = P_i - P_o = C \frac{RT}{P_i A_i^2} \dot{m}^2 \tag{5}$$

where A_i is the cross-sectional area of the tubing, $R = 8.314$ J/(mol·K) is the universal gas constant, T is the gas temperature in kelvins (assumed to be room temperature $T = 293$ K), and C is a fitting constant. This resistance should only depend on the pneumatic hardware, which is kept consistent between tests and designs. The fluidic capacitance, on the other hand, is equivalent to the output pressure within the pouch: $F_{\text{cap}} = P_o$. Since the pouch is inextensible, the pouch pressure is a piecewise function, equal to atmospheric pressure until the pouch reaches its maximum volume given the geometric constraints:

$$P_o = \begin{cases} P_{\text{atm}} & \text{if } m < \frac{P_{\text{atm}} V_{\text{max}}}{RT} \\ \frac{mRT}{V_{\text{max}}} & \text{if } m \geq \frac{P_{\text{atm}} V_{\text{max}}}{RT} \end{cases} \tag{6}$$

where P_o is the pouch pressure, P_{atm} is atmospheric pressure, and V_{max} is the maximum pouch volume given the constraints. For the majority of situations, we will only consider the case where the pouch reaches its full volume. For this reason, the dynamic function is:

$$P_i = C \frac{RT}{P_i A_i^2} \dot{m}^2 + \frac{RT}{V_{\text{max}}} m \tag{7}$$
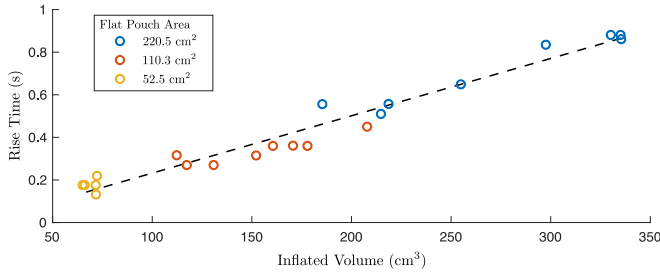
Fig. 5. Measured rise time as a function of the pouch volume. The pouch volume is found by fitting the dynamic model. Rise time is primarily a function of the pouch size.

which can be rewritten in terms of the magnitude of the mass flow rate as:

$$|\dot{m}| = \sqrt{\frac{P_i A_i^2}{CRT} \left| P_i - \frac{RT}{V_{\max}} m \right|} \qquad (8)$$

Since we only measure pressure within the system, we rewrite these dynamics in terms of the output pressure, P_o:

$$\dot{P}_o = \text{sign}(P_i - P_o) \sqrt{\frac{P_i RT}{V_{\max}^2} \frac{A_i^2}{C} |P_i - P_o|} \qquad (9)$$

B. Single Pouch Results

For single pouches, the dynamics were measured after varying pouch size and inflation height. In each test, the pouch was inflated to approximately 10 kPa above atmospheric pressure and the pressure within the pouch was measured over time. Two parameters were extracted from this data: 1) the 10% to 90% rise time and 2) the volume, using the model in (9). Since the resistive parameter, $\frac{A^2}{C}$, cannot be separated from the capacitive parameter, V, when only the pressure is measured, we also measured the volume and dynamic behavior of unconstrained pouches at each size and used those measurements to fit the fluidic resistance, which should be constant across the tests. For three pouch sizes, the volume of the unconstrained pouches was 598 cm³, 244 cm³, and 72.3 cm³ with rise times of 1.76 s, 0.40 s, and 0.27 s, respectively, leading to a $\frac{A^2}{C}$ value of 0.406.

Fig. 5 shows the results of the height-constrained single pouch tests. The rise time for a given pressure increases linearly with the increase in volume. While inflation height has an effect on the volume and, as a result, on the rise time, the pouch area has a much larger effect. As shown in Section II, for a single pouch, contact area can only be increased by changing the pouch size, so this demonstrates a considerable trade off between contact area and dynamic response.

C. Stacked Pouches Results

In the stacked case, the dynamic response depends heavily on how the distal pouch is controlled. Two simple control methods are set mass, where the mass of air within the distal pouch is set before the proximal pouch is pressurized, and set pressure, where the distal pouch pressure is controlled. We will only consider the set pressure control method to
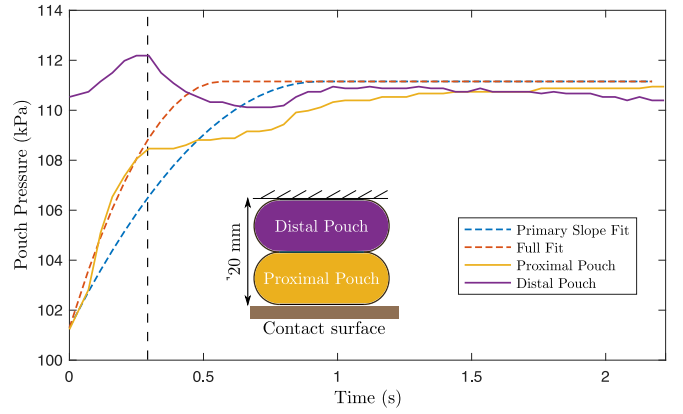

Fig. 6. Behavior of a stacked pouch system with medium pouches inflated to $h = 20$ mm. The distal pouch is controlled to a set pressure and the proximal pouch is given a step input to 10.0 kPa. The dynamic model is fit for the full data set ($V = 290$ cm³, $t_{\text{rise}} = 1.1$ s) and for just the initial slope ($V = 177$ cm³, $t_{\text{rise}} = 0.39$ s).

examine changes in the dynamics. For this, closed-loop pressure control was accomplished using a pressure regulator.

Same-sized and differently-sized stacked pouches were considered. In general, stacking pouches leads to initial rise times that are faster than or equal to single pouches with the same height. In the case of two equal-sized pouches with a flat area of 110.3 cm² (Fig. 6), the initial rise of the proximal pouch pressure leads to a fit with a volume and estimated rise time that are on the lower end of the medium sized pouch grouping in Fig. 5. However, the full rise is much slower after the distal pouch control responds, leading to an undershoot in the distal pouch pressure. This again indicates that stacked dynamics are highly dependent on the control of both pouches. Even in this case though, the change in contact area due to the distal pouch pressure means that the force rise is much faster and the final force is higher.

V. APPLICATION

We created a pneumatic haptic display with adjustable contact area and the fast rise times characteristic of smaller volume pouches. Our stacked pouch array was designed to match data collected during interaction with a teleoperated bimanual robot consisting of two torque-controlled Franka Emika 7-DOF arms and a soft, padded exterior instrumented with 61 force sensors across its chest, back, and arms. In previous work, participants were asked to hug the robot while receiving a teleoperated hug, and the force sensors recorded time series data of the human hugs [19]. Other investigations of robots hugging humans reflect the importance of interpersonal touch and embodied interactions [20], [21].

Due to the robot's teleoperated nature and physical human-robot interaction intrinsic to hugging, a large distributed pressure haptic display could provide useful feedback for a user. Pneumatic actuation is particularly well suited for human-human contact due to the frequency range of volitional human motion being ≤10 Hz [22]. Fig. 7(A) shows a stacked pouch array consisting of one large distal pouch (10.5 cm×21 cm) and four smaller proximal pouches
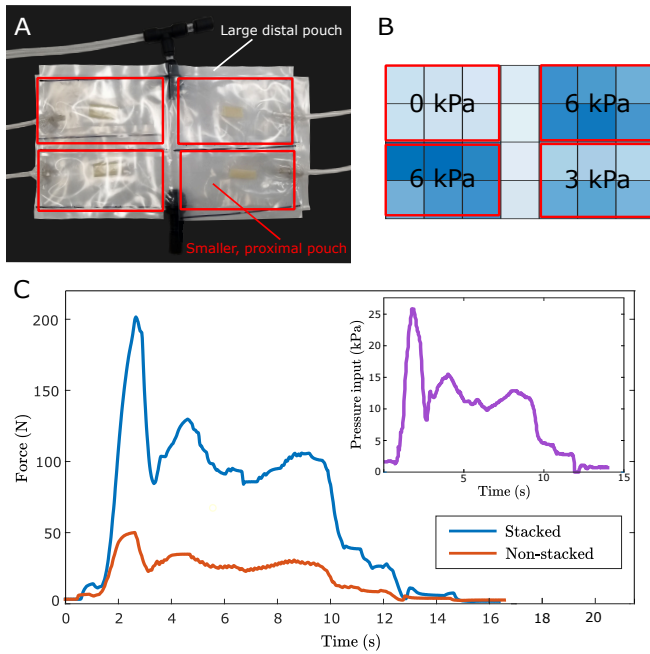
Fig. 7. (A) A pouch array can be constructed by stacking a number of smaller proximal pouches outlined in red beneath one larger distal pouch. (B) This can yield distinct, complex pressure patterns. (C) Depending on whether a stacked or non-stacked configuration is used, the same pressure input signal (obtained from experiments with a huggable robot and shown as an inset in the top right) results in different levels of total applied force.

(5.25 cm×10 cm), which could form one unit of a larger haptic display. By inflating the large distal pouch, the contact area of the smaller pouches for a given height is greater than if they were arranged in parallel by themselves. Controlling each of these smaller pouches individually produces unique pressure patterns (Fig. 7(B)).

We used this stacked pouch array to match pressure profiles from the huggable robot dataset. An Arduino Mega microcontroller commanded recorded pressure profiles to QB3 pressure regulators (Proportion Air). For storage efficiency, these profiles were decomposed into a piecewise function of high order polynomials. Fig. 7(C) shows the total force produced by the stacked pouch setup replicating one such pressure pattern. The same pressure pattern was used as the input for both stacked and non-stacked systems. Stacked pouches yielded a larger total force compared to the non-stacked case due to larger contact area; this difference in total force may elicit different user responses. Moreover, the pouch contact area can be controlled between that of the stacked and non-stacked cases, so this pressure profile can be used to create force profiles between the two extremes in Fig. 7(C).

VI. DISCUSSION AND CONCLUSION

Pressure displays offer a new opportunity for wearable haptic devices, giving the potential to replicate large area interactions. In this work, we showed how the static and dynamic response of inextensible pouches can be modified by stacking equal- or different-sized pouches over the same area of interaction, effecting a macro-mini design strategy.

In analyzing these pouch behaviors in the single and stacked configurations, we showed the importance of considering not only total force but also contact area when describing the generated signals from pressure displays. Single pouch behavior can be described as a function of its geometry as well as its inflation height constraint. With this framework, we showed that stacking pouches was equivalent to modifying the height constraint, giving an extra degree of control.

Compared to a single layer of small pouches, the macro-mini approach of stacking pouches enables the control of contact area within a larger range, and specifically allows a higher maximum contact area than would occur with a single pouch for a given height constraint. The latter is particularly notable since small pouches alone inherently have a limited inflation height while larger pouches limit the system dynamics. Compared to a single large pouch, this approach enables finer resolution of localized forces to be displayed and quicker dynamic response. Both of these allow a larger range of haptic sensations to be rendered. Furthermore, by controlling the effective height in a stacked pouch configuration, the spatial pressure distribution could be dynamically varied with time.

Control of effective pouch height may also allow a potential wearable haptic display to better conform to the human body. Rognon et al. characterized the tolerance of different regions of the upper body to loads produced by a soft exoskeleton and discussed the competing needs to allow for user freedom of motion while ensuring a tight fit between the exoskeleton and the skin to avoid slipping [23]. A pressure-based display with stacked pouches could allow for larger tolerances between the display and the human body without sacrificing contact area, allowing better fit across users. Future work will focus on two aspects of this actuator design: improving models of the pouch interaction and integrating stacked pouch actuators into a wearable haptic design. While most interactions are explained by the simplified behavior described in this paper, some interactions between pouches in a stack are not well accounted for. The stacked pouch model can be improved by modeling the membrane shape at the point of the interaction and better accounting for the volume maximization constraint using techniques like calculus of variations.

Other future work will integrate the stacked pouch design into a wearable haptic system. Important considerations include the control method for the stacked conditions and understanding how the pressure and force responses change when interacting with the compliant surface of the human body. We will also investigate changing pouch geometry to accommodate curved surfaces. We anticipate that such a system is well suited for replicating social touches; volitional human motion frequencies match well with pneumatic actuator bandwidth and this system could be augmented with other actuators (e.g. vibration) for high-frequency contacts. With these improvements, pressure displays can bring new dimensions to wearable haptic devices and better reflect the breadth of haptic interactions in our lives.

REFERENCES

[1] L. A. Jones, M. Nakamura, and B. Lockyer, "Development of a tactile vest," in *International Symposium on Haptic Interfaces for Virtual Environment and Teleoperator Systems*, 2004, pp. 82–89.

[2] R. W. Lindeman, R. Page, Y. Yanagida, and J. L. Sibert, "Towards full-body haptic feedback: The design and deployment of a spatialized vibrotactile feedback system," in *ACM Symposium on Virtual Reality Software and Technology*, 2004, p. 146–149.

[3] F. Gemperle, N. Ota, and D. Siewiorek, "Design of a wearable tactile display," in *International Symposium on Wearable Computers*, 2001, pp. 5–12.

[4] F. Arafsha, K. M. Alam, and A. E. Saddik, "EmoJacket: Consumer centric wearable affective jacket to enhance emotional immersion," in *International Conference on Innovations in Information Technology*, 2012, pp. 350–355.

[5] L. Bonanni, C. Vaucelle, J. Lieberman, and O. Zuckerman, "TapTap: A haptic wearable for asynchronous distributed touch therapy," in *CHI Extended Abstracts on Human Factors in Computing Systems*, 2006, p. 580–585.

[6] P. B. Shull and D. D. Damian, "Haptic wearables as sensory replacement, sensory augmentation and trainer–a review," *Journal of Neuroengineering and Rehabilitation*, vol. 12, no. 1, p. 59, 2015.

[7] A. Delazio, K. Nakagaki, R. L. Klatzky, S. E. Hudson, J. F. Lehman, and A. P. Sample, "Force Jacket: Pneumatically-actuated jacket for embodied haptic experiences," in *CHI Conference on Human Factors in Computing Systems*, 2018, p. 1–12.

[8] C. Rognon, M. Koehler, C. Duriez, D. Floreano, and A. M. Okamura, "Soft haptic device to render the sensation of flying like a drone," *IEEE Robotics and Automation Letters*, vol. 4, no. 3, pp. 2524–2531, 2019.

[9] N. Agharese, T. Cloyd, L. H. Blumenschein, M. Raitor, E. W. Hawkes, H. Culbertson, and A. M. Okamura, "HapWRAP: Soft growing wearable haptic device," in *IEEE International Conference on Robotics and Automation*, 2018, pp. 5466–5472.

[10] J. K. S. Teh, A. D. Cheok, R. L. Peiris, Y. Choi, V. Thuong, and S. Lai, "Huggy Pajama: A mobile parent and child hugging communication system," in *International Conference on Interaction Design and Children*, 2008, p. 250–257.

[11] R. Niiyama, X. Sun, C. Sung, B. An, D. Rus, and S. Kim, "Pouch motors: Printable soft actuators integrated with computational design," *Soft Robotics*, vol. 2, no. 2, pp. 59–70, 2015.

[12] J. D. Greer, T. K. Morimoto, A. M. Okamura, and E. W. Hawkes, "Series pneumatic artificial muscles (sPAMs) and application to a soft continuum robot," in *IEEE International Conference on Robotics and Automation*, 2017, pp. 5503–5510.

[13] I. Sardellitti, J. Park, D. Shin, and O. Khatib, "Air muscle controller design in the distributed macro-mini (DM^2) actuation approach," in *International Conference on Intelligent Robots and Systems*. IEEE, 2007, pp. 1822–1827.

[14] A. C. Robin, "Paper bag problem," *Mathematics Today*, vol. 40, pp. 104–107, 2004.

[15] J. D. Paulsen, "Wrapping liquids, solids, and gases in thin sheets," *Annual Review of Condensed Matter Physics*, vol. 10, no. 1, pp. 431–450, 2019.

[16] I. Pak and J.-M. Schlenker, "Profiles of inflated surfaces," *Journal of Nonlinear Mathematical Physics*, vol. 17, no. 02, pp. 145–157, 2010.

[17] N. S. Usevitch and A. A. Stanley, "Cutting the cord: Soft haptic devices without a pressure source," in *IEEE International Conference on Soft Robotics*, 2019, pp. 49–55.

[18] D. C. Rennels and H. M. Hudson, *Pipe flow: A practical and comprehensive guide*. John Wiley & Sons, 2012.

[19] J. Campbell and K. Yamane, "Learning whole-body human-robot haptic interaction in social contexts," in *IEEE International Conference on Robotics and Automation*, 2020, pp. 10 177–10 183.

[20] M. Jindai, S. Ota, T. Yasuda, and T. Sasaki, "Hug behavior request model with approaching human for hug robots," in *Social Robotics*, M. A. Salichs, S. S. Ge, E. I. Barakova, J.-J. Cabibihan, A. R. Wagner, Á. Castro-González, and H. He, Eds. Cham: Springer International Publishing, 2019, pp. 247–255.

[21] A. E. Block and K. J. Kuchenbecker, "Softness, warmth, and responsiveness improve robot hugs," *International Journal of Social Robotics*, vol. 11, no. 1, pp. 49–64, 2019.

[22] T. L. Brooks, "Telerobotic response requirements," in *1990 IEEE international conference on systems, man, and cybernetics conference proceedings*. IEEE, 1990, pp. 113–120.

[23] C. Rognon, S. Mintchev, F. Dell'Agnola, A. Cherpillod, D. Atienza, and D. Floreano, "FlyJacket: An upper body soft exoskeleton for immersive drone control," *IEEE Robotics and Automation Letters*, vol. 3, no. 3, pp. 2362–2369, 2018.